

MEG, myself, and I: individual identification from neurophysiological brain activity

Jason Da Silva Castanheira^{1,*}, Hector D Orozco^{1,2,*}, Bratislav Misic^{1,†}, Sylvain Baillet^{1,†}

¹ Montreal Neurological Institute, McGill University, Montreal QC, Canada

² Department of Psychology, Neuroscience, and Behavior, McMaster University, Hamilton ON, Canada

* Contributed equally.

† Corresponding authors: bratislav.misic@mcgill.ca, sylvain.baillet@mcgill.ca.

Abstract

Large, openly available datasets and current analytic tools promise the emergence of population neuroscience. The considerable diversity in personality traits and behaviour between individuals is reflected in the statistical variability of neural data collected in such repositories. This variability challenges the sensitivity and specificity of analysis methods. Yet, recent studies with functional magnetic resonance imaging (fMRI) have concluded that patterns of resting-state functional connectivity can both successfully identify individuals within a cohort and predict their individual traits, yielding the notion of a *neural fingerprint*. Here, we aimed to clarify the neurophysiological foundations of individual differentiation from features of the rich and complex dynamics of magnetoencephalography (MEG) resting-state brain activity in 158 participants. The resulting neurophysiological functional connectomes enabled the identification of individuals with similar identifiability rates to fMRI. We also show that individual identification was equally successful from simpler measures of the spatial distribution of neurophysiological spectral signal power. Our data indicate that identifiability can be achieved from brain recordings as short as 30 seconds, and that it is robust over time: individuals remain identifiable from recordings performed weeks after their baseline reference data was collected. We can anticipate a vast range of diverse applications in personalized, clinical and basic neuroscience of individual differentiation from large-scale neural electrophysiology, in future longitudinal and cross-section studies.

Introduction

Understanding the biological nature of individual traits and behaviour is an overarching objective of neuroscience research (1–4). The increasing availability of large, openly available datasets and advanced computational tools propels the field toward this aim (5–7). Yet, with bigger and deeper data volumes, neuroscientists approach a paradox: while big-data neuroscience approaches the realm of population neuroscience, we remain challenged by understanding how interindividual data variability echoes the singularity of the self (1, 3, 8, 9).

This epistemological question has become particularly vivid with recent research showing that individuals can be identified from a cohort via their respective *neural fingerprints*, derived from structural magnetic resonance imaging (MRI) (10, 11), functional MRI (fMRI) (12–16), electroencephalography (EEG) (17, 18), or functional near-infrared spectroscopy (fNIRS) (19). Strikingly, neural fingerprints are associated with individual traits such as global intelligence, working memory, and attention abilities (20–23). Most published work so far is methodologically based on inter-individual similarity measures of functional connectivity—understood as statistical dependencies between ongoing signals across brain regions in task-free awake conditions (24, 25)—as defining features of neural fingerprints. Yet, the indirect coupling between hemodynamic and neural brain signaling interrogate the neurophysiological nature of brain fingerprints. Previous EEG fingerprinting work was restricted to scalp data, and therefore, provided limited neuroanatomical insight.

In electrophysiology indeed, ongoing brain dynamics at rest are rich and complex (Baillet, 2017) and have long been considered a nuisance, a by-product of neural noise (27–29). Recent experimental evidence, spurred by systems neuroscience models, indicates that spontaneous brain activity captured using electrophysiological techniques expresses similar resting-state connectomes as fMRI and influences conscious, sensory processes (30–32). Ongoing neurophysiological activity varies considerably between individuals and across the lifespan. One instance is the inter-individual variability of prominent features of human brain neurophysiological activity, such as the alpha rhythm (8–12 Hz) peak frequency (33, 34). Overall, the unique signature components of fast, neurophysiological brain dynamics across individuals remain uncharted.

Here we used resting state recordings of magnetoencephalography (MEG; Baillet, 2017) from a large cohort of participants to identify neurophysiological features of individual differentiation. We derived both measures of functional organization (i.e., functional connectivity) inspired by fMRI *neural fingerprinting* approaches, and spectral signal markers that are proper to the wider frequency spectrum of brain signaling accessible to neurophysiological data.

Results

We used MEG data from 158 participants available from the Open MEG Archives (OMEGA; Niso et al., 2016). Data collected on multiple days were available for a subset of these participants (N=47; mean duration between consecutive sessions: 201.8 days; Figure 1). The participants were both healthy and patient volunteers (ADHD and chronic pain) spanning in age from 18 – 73

years-old (see Supplemental Material). T1-weighted structural MRI volumes were available from OMEGA for all participants and were used to produce source maps of resting-state brain activity (Baillet et al., 2001). We derived several neurophysiological signal features from MEG brain source time series summarized within the Desikan-Killiany atlas—68 regions of interest (ROIs) parcellating the entire cortical surface (36). The MEG features comprised power-spectral-density, spectral estimates (PSD) within each ROI across 68 regions of interest (ROIs; Desikan et al., 2006), and 68x68 functional connectomes (FC) between ROIs. The approach is summarized graphically Figure 1 and the FC and PSD methodological details are provided in Materials and Methods.

Participant identification was performed across pairs of MEG data segments taken from either the same (*within-session* identification) or a repeated session (*between-session* identification) using two distinct datasets (Figure 1a), using either FC or PSD features (referred as *connectome* and *spectral* fingerprinting, respectively). For each pair of participants, the Pearson’s correlation coefficient between their respective features (i.e., FC or PSD) was the corresponding entry in the group correlation matrix. The identification procedure for each individual proceeded via a lookup operation through the corresponding row of the correlation matrix; the index of the column featuring the largest correlation coefficient determined the predicted identity of the individual in the cohort. Thus, if a given individual’s data features from the first dataset were most correlated to the data features from their second dataset, the individual would be correctly identified. Note that taking the maximum along the rows or columns simply switches which dataset is used for deriving the identification features (e.g., identifying individuals using dataset 1 from features derived from dataset 2; results for all possible combinations of datasets are in Supplemental Material). The overall accuracy of the identification procedure was computed as the proportion of participants correctly identified. We ran three types of identification challenges: *within-session* identification consisted of the personal differentiation between 158 participants (i.e., the datasets were from same-day recordings split in half); *within-session* identification using considerably shortened data segments (30 seconds from 175 seconds); and a *between-session* identification challenge for a subset of 47 participants for whom the datasets were from two separate days (Figure 1a). We conducted the identification challenges using either broadband MEG data or band-limited versions within the typical frequency bands used in neurophysiology. We also derived a self-identifiability score for every participant, which indicates the saliency of the identification of any given individual in the tested cohort (see Material and Methods).

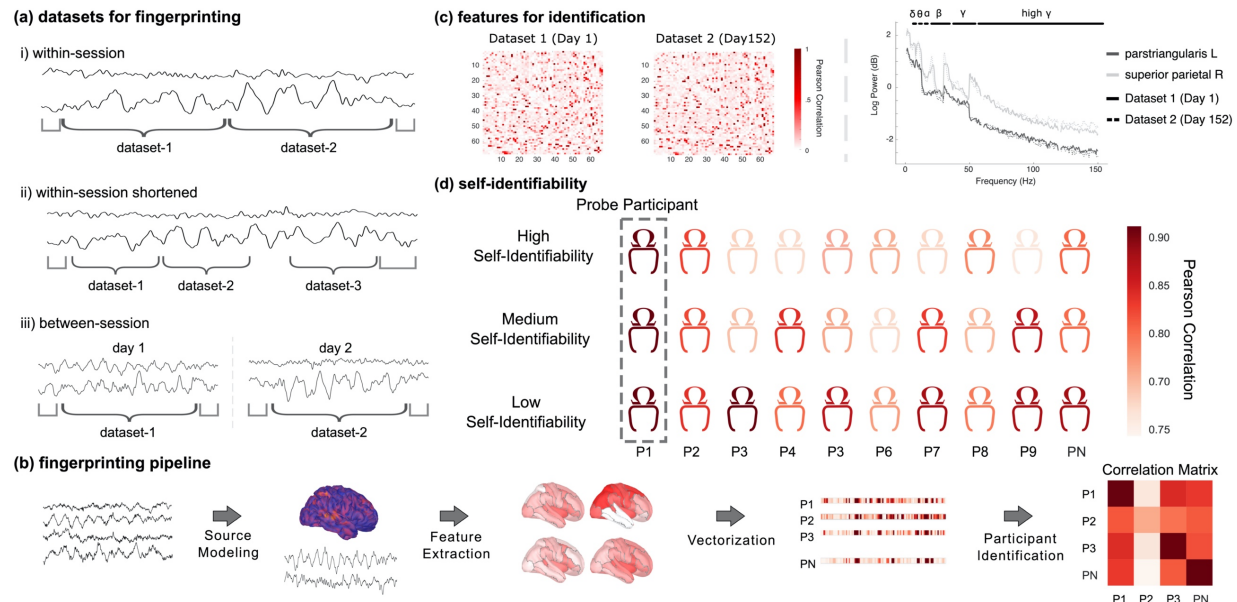


Figure 1: Identification analysis pipeline and definition of self-identifiability

(a) Schematic of exemplar MEG data divided into datasets for each of the specified analyses. In the *i) within-session* analysis we split each session volume in half, in the *ii) within-session shortened* analysis we similarly split the session volume into three 30-second segments, and lastly in the *iii) between-sessions* analysis used data recorded on two separate days. (b) Schematic of the data analysis pipeline: source modeling was first performed before extracting features from each region of the Desikan-Killiany atlas (36). These features were vectorized and subsequently used to fingerprint individuals, yielding a participant correlation matrix. (c) Features for the *between-session* challenge from an exemplar subject. Left panel depicts AEC functional connectivity matrices across two datasets; both matrices feature the Pearson correlation coefficients between all regions of the Desikan-Killiany atlas (36). Right panel plots the power spectrum density estimates from two regions of the atlas, across two datasets. (d) Self-identifiability was derived for each participant as the z-score of their correlation to themselves, relative to the correlation between themselves and the rest of the cohort. A participant with a high correlation to themselves and low correlations to others was qualified as *highly identifiable*. An individual highly correlated to both themselves and many others in the cohort was qualified as *less identifiable*.

Within-session, connectome and spectral data, differentiate individuals

Within-session MEG connectome and spectral fingerprinting achieved 94.9% and 96.2% participant identification accuracy, respectively (Figure 2). This outcome was robust to switching datasets (Supplemental Material). While previous work (12) reported that data reduction strategies improved identification performances, this was not the case with our data. Data reduction strategies only marginally improved individual differentiation, as explained in Supplemental Material.

We also ran the identification procedure across the typical frequency bands of electrophysiology to understand whether the expression of certain ranges of brain rhythms would be more specific

of individual differentiation. We bandpass filtered MEG signals in the delta (1-4Hz), theta (4-8Hz), alpha (8-13Hz), beta (13-30Hz), gamma (30-50Hz) and high gamma (50-150Hz) frequency bands before running the same *within-session* fingerprinting procedure with resulting narrowband signals. Narrowband connectome fingerprinting yielded identification accuracy scores of 98.7% for delta, 100% for theta, 99.4% for alpha, 100% for beta, 98.7% for gamma, and 94.9% for high gamma. Narrowband spectral fingerprinting produced identification accuracies of 94.9% for delta, 95.6% for theta, 95.6% for alpha, 96.2% for beta, 96.2% for gamma, and 97.5% for high gamma. These results are summarized Figure 2a.

We further challenged MEG individual differentiation using shorter, 30-second data segments. We extracted three 30-second segments from the *within-session* data (Figure 1a) and ran the same fingerprinting procedures as above. Identification accuracy with connectome fingerprinting was not affected substantially (94.9%, 93.7%, and 96.8% across all tested 30-second segments; Figure 2) using broadband MEG signals. However, spectral fingerprinting was strongly degraded by using shorter data segments (identification accuracy: 62.7%, 71.5%, and 90.5%; Figure 2). We observed similar discrepancies in performance robustness between connectome and spectral fingerprinting using narrowband signals (Figure 2), especially in the delta, theta, and alpha bands. We also observed that using data segments collected closer in time yielded higher identification accuracies i.e., using features from the first dataset to identify individuals from data in the second dataset outperformed fingerprinting when the first dataset was used to identify participants from data in the third, more distal in time, dataset. We report identification accuracies for all possible combinations of dataset pairs in Supplemental Material.

MEG fingerprinting is robust against physiological, artefactual, and demographics confounds

We investigated the robustness of these results against variables of no interest and possible confounds. We performed Pearson correlation analyses between identification scores and recording parameters, typical MEG artifacts and demographic variables. There was no association between the duration of scans and self-identifiability for connectome ($r=-0.02$, $p=0.75$) and spectral ($r=0.02$, $p=0.8$) fingerprinting (Supplementary Material). Further, none of the tested MEG artifacts due to eye movements, heartbeats and head motion were related to individual identifiability across both connectome and spectral fingerprinting. Indeed, self-identifiability was not correlated to motion (connectome: $r=0.06$, $p=0.5$; spectral: $r=-0.01$, $p=0.9$), cardiac (connectome: $r=0.05$, $p=0.6$; spectral: $r=0.07$, $p=0.4$), or ocular (connectome: $r=-0.09$, $p=0.3$; spectral: $r=-0.05$, $p=0.5$) artifacts (Figure 2b). We further hypothesized that fingerprinting performances may have been skewed by sample heterogeneity in terms of data from healthy vs. patient participants. Yet, there was less than 1% differences in identification accuracy after restricting fingerprinting to healthy participant data (Supplemental Material). We also verified that participant demographics such as age, sex, and handedness did not contribute to identifiability either (Supplemental Material).

164

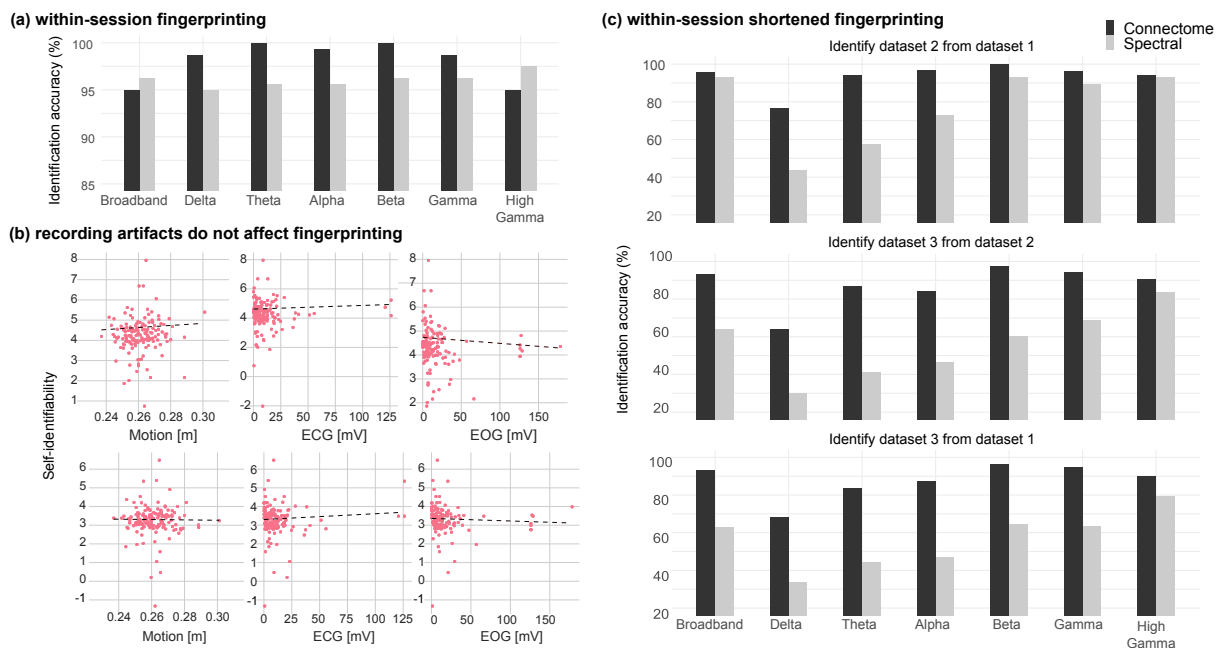


Figure 2: Within-session identification accuracy, unrelated to artifacts

(a) identification accuracy of connectome and spectral fingerprinting across the broad- and narrow-band scouted time series for the *within-session* identification challenge. Connectome and spectral fingerprinting have similar performances on broadband data. Connectome fingerprinting performed better with theta, alpha, and beta narrowband data. In contrast, spectral fingerprinting performance was qualitatively similar across frequency bands. **(b)** Self-identifiability was not related to head motion, eye-movements or heartbeat artifacts (top row connectome, bottom row spectral fingerprinting). **(c)** identification accuracy for the *within-session shortened* analysis. Connectome outperformed spectral fingerprinting, especially when datasets were farther apart in time (i.e., datasets 1 and 3).

MEG fingerprinting is robust over time

We tested whether participants who underwent MEG sessions on separate days were identifiable from datasets collected weeks to months apart (with a range of 1 – 1029 days apart and an average of 201.7 days, SD=210.1). We applied the above fingerprinting procedures towards this *between-session* challenge on the subset of participants concerned (N=47). Connectome fingerprinting decreased in performance compared to the identification accuracy scores obtained from the *within-session* challenge (89.4%). Performance of connectome fingerprinting from narrowband signals also decreased, with the greatest robustness obtained from using signals in the beta and theta bands (Figure 3 and Supplemental Material). In contrast, spectral fingerprinting was robust longitudinally, with identification accuracy scores of 97.9% (broadband) and >90% (narrowband) that were similar to those obtained in the *within-session* challenge (Figure 3 and Supplemental Material). Self-identifiability scores were not correlated

with the number of days between MEG sessions (connectome: $r = 0.09$, $p = 0.5$; spectral: $r = 0.08$, $p = 0.65$).

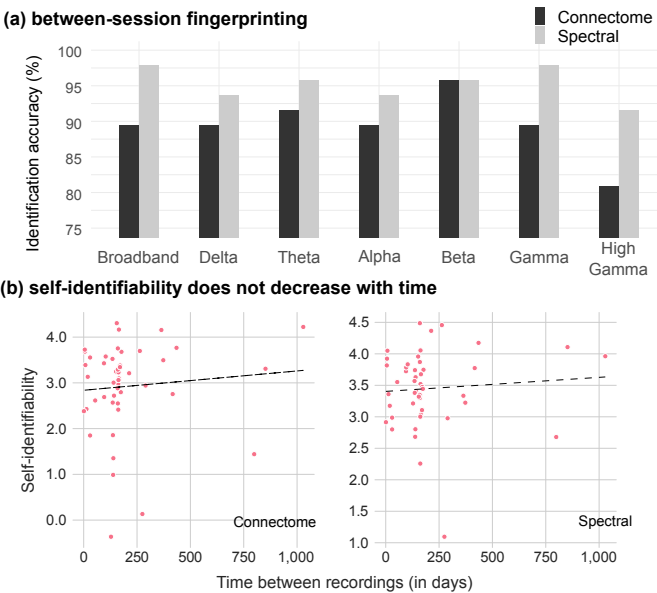


Figure 3: Between-session identification accuracy

(a) Identification accuracy for connectome and spectral *between-session* fingerprinting. Performances were similar to those from the *within-session* challenge, especially for spectral fingerprinting, which remained accurate with broad- and narrow-band data. **(b)** Linear regression analyses did not reveal an association between self-identifiability and the duration between recordings, in days (connectome: $r = 0.09$, $p = 0.5$; spectral: $r = 0.08$, $p = 0.65$).

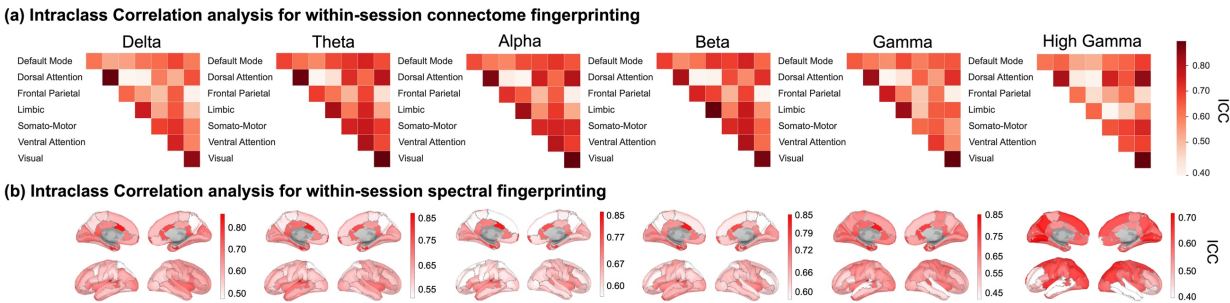


Figure 4: Characteristic features for connectome and spectral fingerprinting

Intra-Class Correlation (ICC) for connectome and spectral *within-session* fingerprinting. **(a)** ICC for connectome fingerprinting plotted across each frequency band, with network/region labelling according to Yeo et al. (2011): Default Mode Network (DMN), Dorsal Attention (DA), Frontal-Parietal (FP), Limbic (L), Somato-Motor (SM), Ventral Attention (VA), and Visual (VIS). The most prominent connection features for connectome fingerprinting were the Visual, Dorsal Attention and Limbic networks. **(b)** ICC for spectral fingerprinting plotted for each tested frequency band,

using the Desikan-Killiany cortical parcellation (36). The most salient features included Gamma and High-Gamma band signals in midline structures.

Salient neurophysiological features for identification

We identified the features which were the most characteristic of individuals for MEG fingerprinting. We derived measures of intraclass correlation (ICC) (12) to quantify how much each feature, such as an edge of the FC connectome or a frequency band in an anatomical parcel, contributed to fingerprinting (see Methods). This metric used in previous brain fingerprinting studies captures the inter-rater reliability of each participant as their own rater, to identify the edges which neurophysiological signal features are the most consistent across individuals (12, 37). We performed analysis separately for the broadband connectome and spectral fingerprinting *within-session* challenges. The data show that the dorsal attention and visual networks were the most specific across individuals for connectome fingerprinting, across all frequency bands. These results also highlight that the theta, alpha and beta bands stand out in their ability to distinguish individuals, with an emphasis on limbic beta connectivity (Figure 4). Activity in medial regions across all bands stood out in the identification of individuals using spectral fingerprinting (Figure 4b). Particularly, signals in the gamma and high-gamma bands discriminated individuals along midline, parietal, and visual areas, which was consistent with the narrowband results above.

Neurophysiological identifying features are associated with demographics

Beyond identifying individuals in a cohort, we tested whether resting-state neurophysiological signals could predict meaningful participant traits using an exploratory partial-least-squares (PLS) analysis (see Methods). Briefly, PLS explains the covariance between two observation matrices – here a demographic matrix with a neurophysiological signal matrix (from ROI-specific PSD or FC measures) – based on latent components. Our data pointed at three significant latent components, which were distinct for connectome and spectral fingerprinting (Supplemental Material). The first latent component in connectome fingerprinting was related to clinical population ($r = 0.2$, 95% CI [0.160, 0.3]) and handedness ($r = 0.2$, 95% CI [0.1, 0.3]). This demographic profile was associated with reduced beta-band functional connectivity over the frontal parietal network (Figure 5). For PSD fingerprinting, the first salient latent component was related to a younger age ($r = -0.3$, 95% CI [-0.1, -0.5]), female ($r = 0.4$, 95% CI [0.2, 0.5]) and clinical population ($r = 0.5$, 95% CI [0.2, 0.5]). This demographic profile was associated with stronger expressions of broadband neurophysiological signal power in superior parietal regions and the pericalcarine gyrus bilaterally and reduced neurophysiological signals in the isthmus cingulate (Figure 5).

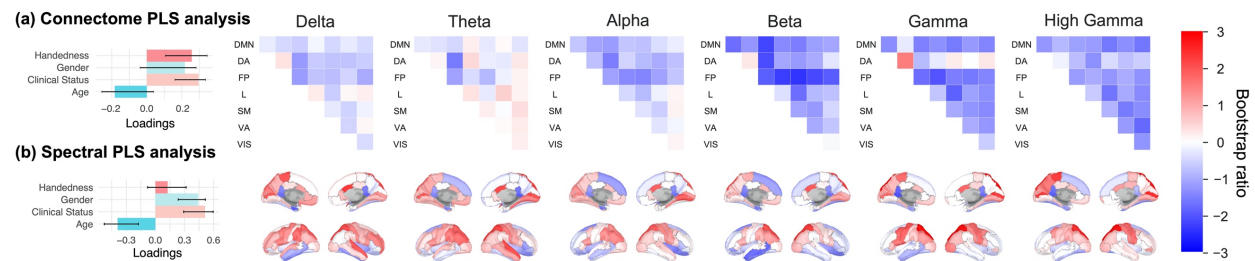


Figure 5: Partial Least-Squares analysis relates demographics to connectome and spectral features

(a) and (b) from left to right, depicts the design saliency patterns for the first latent variables and their associated neural-data bootstrap ratios. Confidence Intervals (CI) are calculated through a bootstrapping procedure, and as such may not necessarily be symmetric. Bootstrap ratios computed for connectome (a) and spectral features (b) and plotted according to resting-state networks derived by (Yeo et al., 2011) and the Desikan-Killiany atlas (36) respectively.

Discussion

The recent leveraging of large, open fMRI datasets has brought empirical evidence that individuals may be identified within a cohort from their brain imaging functional connectome, inspiring the metaphor of a *neural fingerprint*. Unlike hand fingerprints, their cerebral counterpart predicts task performance and a variety of traits (14, 20–23). These intriguing findings require a better understanding of their neurophysiological foundations, which we sought to characterize from direct neural signals captured at a large scale with MEG. Our data show that individuals can be identified in a cohort of 158 unrelated participants from their respective resting-state connectomes and spectral profiles in a range of fast brain signals. MEG fingerprinting was successful using data lengths (30 seconds) much shorter than those reported for fMRI fingerprinting (14, 39). Brain electrophysiological signals are rich, complex, and convey expressions of large-scale neural dynamics channeled by individual structural anatomy and physiology (40). Indeed, we also showed that MEG fingerprinting is robust across time, making individuals potentially identifiable from data collected days, months or years apart. Lastly, we characterized whether individual differences in resting-state neural dynamics are meaningful through an exploratory PLS analysis. We showed that both resting-state functional connectomes and spectra predict latent demographic components. Recent findings corroborate our results, demonstrating meaningful individual differences between functional connectomes derived from resting-state electrophysiology (41).

Connectome and spectral neurophysiological fingerprints

Our results highlight two sets of brain-wide electrophysiological features that contributed to successful individual identification: connectome and spectral measures across the neurophysiological frequency spectrum. Overall, connectome and spectral fingerprinting with MEG performed equivalently to fMRI approaches, achieving overall identification rates above 90%, with robust individual identification over time and against noise (12, 14, 42).

We found that for connectome fingerprinting, the anatomical regions the most characteristic of individuals differed between MEG and fMRI. While fMRI highlighted the default-mode network and the fronto-parietal resting state networks, MEG connectome fingerprinting emphasized functional connectivity within limbic and visual networks as contributing to individual specific neurophysiological signatures. In contrast, both MEG and fMRI fingerprinting emphasize the importance of the dorsal attention network (14). These observations are not mutually exclusive, considering the different nature of brain signals captured by the respective modalities. One possible interpretation—requiring further investigation— is that the fast neurophysiological signals that contribute to identification with MEG have hemodynamic counterparts that are not as salient in fMRI as the identifying networks reported so far. Nevertheless, our data indicate that neurophysiological signals in the beta band contribute to the highest identification accuracy amongst all other typical bands. This finding is compatible with previous work reporting that correlated amplitude changes of MEG brain signals are related to the microstructure of white matter tracts and reveal, with the same amplitude envelope correlation method as used here, MEG resting-state brain networks that align with fMRI’s (43, 44). Beta signalling also emerges from recent literature as a signalling vehicle of re-afferent “top-down” communications in brain signals (45, 46). One can therefore speculate that beta-band signals would convey electrophysiological representations of internal cognitive models that are by essence intimately specific of each individual (Baillet, 2017).

Such brain signal amplitude signatures are further emphasized by the ability of simple spectral brain maps to enable MEG fingerprinting. *Within-* and *between-session* spectral identification were achieved with remarkable accuracy (>90%) with broadband MEG brain signals or restricted to the typical bands of electrophysiology. Spectral identification based on signals from the faster bands (gamma and high-gamma) was overall the most robust longitudinally and against using shorter data segments. This observation is consistent with the width of (high) gamma frequency bands spanning broader ranges (here between 30-50 Hz and 50-150 Hz) than slower bands such as delta (1-4 Hz), theta (4-8 Hz) and alpha (8-12 Hz). The spectral estimates averaged across the broader (high) gamma bands were therefore the most robust against using shorter data segments. The reduced number of sliding time windows available over shorter data durations increased the variance of the spectral summary statistics extracted to derive the spectral fingerprints from the signals defined over narrower bands. The higher frequency bands were less affected because the larger number of frequency bins involved in the extraction of their summary power statistics tended to compensate the higher empirical variance across reduced signal durations. Connectome fingerprinting was more immune against using shorter data durations. The underlying approach indeed did not require spectral transformations but resorted to a bank of narrowband filters applied over the original duration of MEG recordings, before the resulting filtered signals were segmented in shorter epochs for the identification challenges. The consequence is that the number of data points used for all narrowband signals was identical across all frequency bands, yielding moderate variability in identification performances compared to those obtained with the spectral approach. Another factor of robustness of the connectome approach is that connectivity weights between network nodes may fluctuate very slowly over time in task free brain activity: Florin and Baillet (2015) reported fluctuation rates of 0.01Hz in MEG, indicating typical time cycles of 100s — a duration substantially longer than the

30-s shortest time window used here. Over longer periods of time though, such as in the *between-session* challenge, spectral fingerprinting outperformed its connectome counterpart. We note a slight increase of spectral identification accuracy in the *between-session* challenge (e.g., +1.6% for broadband fingerprinting) compared to *within-session*, which was a statistical fluctuation due to using a smaller sample of participants. More broadly, gamma and faster activity has long been associated with concurrent and colocalized hemodynamic fluctuations (47, 48), which underlines why such signals contribute robustly to MEG brain fingerprinting, as dual manifestations of the BOLD signal changes used for fMRI fingerprinting. Gamma-band and faster brain signals are weaker and therefore more prone to contamination from artifacts and noise (49–51). The preprocessing applied to our data attenuated such nuisance to a point where individuals were not identifiable from typical sources of signal contamination such as individual head motion behavior. On average across all fingerprinting challenges, identification using brain signals was overall successful using lower frequency bands (delta 68.8%, theta 79.0%, alpha 80.9%) but was markedly better from high-frequency signal components (beta 91.1%; gamma 89.5%; high gamma 89.0%). Although a rhythm of prominent amplitude in humans during rest, alpha-band activity (8-12Hz) was not particularly specific to identify individuals in the cohort. In that respect, our data is aligned with previous MEG works on resting-state connectomes extracted from neurophysiological MEG signals, which did not report on a salient role of alpha activity in driving inter-regional connectivity (30, 43). We argue that the spatial topography of alpha resting activity may be relatively stereotypical across individuals, involving thalamo-cortical loops that project focally to the parieto-occipital junction, with restricted variability across individuals (6). In task, alpha activity has been related to attention orienting, alertness and anticipation, thereby reflecting transient mental states (39, 52–54) rather than individual traits. While our present data show robust longitudinal fingerprinting performances, future work involving more participants with multiple MEG visits is required to both replicate these observations and investigate whether individual deviations from baseline fingerprints could be early signals of asymptomatic neuropathophysiology (Baillet, 2017). Indeed, we have not addressed how different measures of functional connectivity and spectral power may boost or hinder the ability to identify individuals. Considering this, the remarkable ability to fingerprint individuals with the chosen electrophysiological features serves as a steppingstone for future investigation. Combined fMRI and MEG fingerprinting offers a new avenue for non-invasive endophenotyping.

Neural fingerprints of individual traits

Our data suggests that individual differences in resting-state neurophysiological functional connectivity and spectral power relate to latent demographic clusters. These observations are in line with previous fMRI work that showed that connectomes are predictive of individual differences in attention, working memory and intelligence. For instance, connectivity patterns between the default mode and the dorsal attention networks predict attentional behaviour during task and self-reported mind wandering (Monica D. Rosenberg et al., 2016, 2020, see Rosenberg et al., 2017 for review). Overall, the conceptual framework is that task free neural dynamics are the signatures of an individual scaffold of brain functions that is predictive of task

behaviour. This view is also that of the spontaneous trait reactivation hypothesis wherein the organization of the human cortex at rest (manifested e.g., by functional connectivity) is a window into the self's unique traits and abilities (57). Early evidence indeed suggests that functional connectomes are associated with personality traits and even inter-personal closeness in social networks (58, 59).

Yet, the mechanistic implementation of these intriguing observations remains elusive. Inter-individual variability in the distribution of synaptic weights across the cerebrum, shaped through lifetime experiences according to Hebbian principles, may account — at least in part — for connectome fingerprinting (57). The heritability of the functional connectome has also been discussed, especially for fronto-parietal networks (i.e., DAN, VAN and DMN) (60–62). Heritability of brain spectral characteristics is also actively discussed (63–65). This emerging literature and the empirical evidence of brain fingerprinting certainly motivates more research on new, fascinating questions about the biological nature of the self.

Sampling population diversity for personalized interventions

Robust individual signatures of brain activity have potential to open new possibilities in the domain of neurophysiological endophenotyping and population neuroscience. With the increasing availability of multi-omic data repositories, there is a research opportunity to span the diversity of statistical normative characteristics of brain fingerprints across the population, in relation to behavior and clinical phenotypes (1, 3, 26). Ideally, large databanks of individual variants sampled across multiple dimensions of socio-economic, age, and geographic factors enable normative modeling approaches to establish the risk traits of developing syndromes of e.g., early cognitive decline, neurodegeneration, or mental illness. Brain fingerprints derived from relatively short, task free scanning sessions may play a leading role to realize this vision. Likewise, brain fingerprinting may contribute to future endeavours in establishing how oscillatory dynamics at rest support cognitive functions across the lifespan. MEG brain fingerprinting presents several potential advantages in terms of safety, shorter scan time, and immediate proximity of a care person during data collection, for special populations. The prospect of transferring MEG fingerprinting methodology to EEG as a more accessible sister technology is also appealing.

In sum, our study extends the concept of neural or brain fingerprint to fast and large-scale resting-state electrophysiological dynamics, which encapsulate meaningful individual differences in both functional connectivity and neuroanatomical maps of power spectrum characteristics. We are hopeful that the present contribution paves the way to replication and extension using larger open datasets. Many fascinating outstanding questions remain about the biological nature of inter-individual variability expressed via neural oscillations and brain network dynamics, and more specifically how these differences associate with behavior and diseases natural history. The research ahead is for future population neuroscience studies.

399 Material and Methods

400 The Open MEG Archives (OMEGA)

401 We used data from the Open MEG Archives (OMEGA; Niso et al., 2016) consisting of resting-
402 state MEG recordings acquired using the same MEG system (275 channels whole-head CTF; Port
403 Coquitlam, British Columbia, Canada). The sampling rate was 2400 Hz, with an antialiasing filter
404 applied at 600 Hz cut-off, and built-in third-order spatial gradient noise cancellation (see Niso et
405 al., 2016 for details on data acquisition).

406 We analysed MEG resting-state data from 158 unrelated OMEG participants (77 Females, $31.9 \pm$
407 14.7 years old). Recordings were approximately 5-min long. Supplementary Table 1 provides
408 details on scanning procedures and Supplementary Table 2 on demographics. A subset of these
409 individuals (N=47) had recordings over multiple visits (different days) and were used in the
410 *between-session* fingerprinting challenge. The OMEGA data management protocol was approved
411 by the research ethics board of the Montreal Neurological Institute.

412 MEG data preprocessing and feature extraction

413 MEG data were preprocessed using Brainstorm (Tadel et al., 2011 version Oct-12-2018)
414 (following good-practice guidelines (67). Unless specified, all steps below were performed using
415 the Brainstorm toolkit, with default parameters. Line noise artifact (60 Hz) along with its 10
416 harmonics were removed using a notch filter bank. Slow-wave and DC-offset artifacts were
417 removed using a high-pass FIR filter with a 0.3-Hz cutoff. We derived Signal-Space Projections
418 (SSPs) to remove cardiac and ocular artifacts. We used electro-cardiogram and -oculogram
419 recordings to define signal projectors around identified artifact occurrences. We also applied
420 SSPs to attenuate low-frequency (1-7 Hz) and high-frequency noisy components (40-400Hz) due
421 to saccades and muscle activity, respectively. Bandpass filtered duplicates of the cleaned data
422 were produced for each frequency band of interest (delta: 1-4Hz, theta: 4-8Hz, alpha: 8-13Hz,
423 beta: 13-30Hz, gamma: 30-50Hz, and high gamma: 50-150Hz). Distinct brain source models were
424 then derived for all narrowband versions of the MEG sensor data.

425 Each individual T1-weighted MRI data was automatically segmented and labelled with Freesurfer
426 (68). Coregistration with MEG sensor locations was derived using dozens of digitized head points
427 collected at each MEG session. We produced MEG forward head models for each participant
428 using the overlapping spheres approach, and cortical source models with LCMV beamforming, all
429 using Brainstorm with default parameters (source estimation 2016 version). Elementary MEG
430 source orientations were constrained normal to the surface at 15,000 locations of the cortex.
431 Noise statistics for source modeling were estimated from two-minute empty-room recordings
432 collected as close as possible in time to each participant's MEG session. Source timeseries were
433 clustered into 68 cortical regions of interest (ROIs) defined from the Desikan-Killiany atlas (36)
434 and dimension-reduced via the first principal component of all signals within each ROI.

435 Connectome and spectral identification features were computed from ROI source timeseries.
436 Individual functional connectomes were derived in all frequency bands from the amplitude
437 envelope correlation (AEC) approach (69). ROI timeseries were Hilbert transformed and all
438 possible pairs of resulting amplitude envelopes were used to derive the corresponding Pearson

correlation coefficients, yielding a 68x68 symmetric connectome array. We used Welch's method to derive power spectrum density (PSD) estimates for each ROI (70), using time windows of 2 seconds with 50% overlap sled over all ROI timeseries and averaged across all PSDs within each ROI.

Code Availability

The connectome and spectral features were then exported to Python (3.7.6) for subsequent fingerprinting analyses. All codes for including preprocessing and data analysis can be found on the project's GitHub (LINK).

Data Availability

The power spectra and connectomes derived from the preprocessed OMEGA samples and used to identify individuals in the present study are available upon request from corresponding authors.

Fingerprinting and self-identifiability

We used a fingerprinting approach directly adapted from fMRI connectome fingerprinting methods (12, 14), which relies on correlational scoring of individuals between datasets. A given *probe* participant is identified from a cohort by computing all Pearson correlation coefficients between the spectral or connectome features of said probe at one timepoint (e.g., *dataset 1*) and the entire cohort at a different timepoint (e.g., *dataset 2*). The entry presenting the highest correlation to the probe determined the probe's estimated identity i.e., identified entry in the cohort. This approach is applied between all pairs of participants in the cohort, yielding an asymmetric correlation matrix spanning the cohort. We report scores of *identification accuracy* as the ratio between the number individuals correctly identified with the described procedure and the total number of individuals in the cohort. Identification accuracy scores are obtained from identification challenges from dataset 1 to dataset 2 and vice-versa, *within-* and *between-sessions*. Figure 1 details the definition of the dataset labels used, and Supplemental Material contains the results from across all combinations of datasets/sessions.

Amico and Goñi (2018) proposed an identifiability score to quantify, for a given participant, the reliability of its identification from others in the cohort. Here, we extend this notion with the introduction of a *self-identifiability* measure, I_{self} . Let \mathbf{A} be the correlation matrix spanning the cohort (square, asymmetric) between dataset 1 and dataset 2, and N be the number of participants to identify. We define I_{self} as the z-score of participant P_i 's correlation to themselves between dataset 1 and dataset 2, with respect to P_i 's correlation to all other individuals in the cohort, noted: $I_{\text{self}}(i) = (\text{Corr}_{ii} - \mu_{ij}) / \sigma_{ij}$, where Corr_{ii} is the P_i 's correlation between dataset 1 and dataset 2, μ_{ij} is the mean correlation between participant P_i in dataset 1 and all other individuals in dataset 2 (i.e. the mean along the i^{th} row of matrix \mathbf{A}), and σ_i is the empirical standard deviation of inter-individual features correlations. Thus, if a participant is easily identifiable, its self-identifiability increases; whereas small self-identifiability scores indicate a participant particularly difficult to identify from the rest of the cohort.

Recording artifacts and self-identifiability

To investigate the effects of recording parameters and artifacts on fingerprinting, we related each individual's self-identifiability to several possible confounds. The duration of each scan was compared to self-identifiability to verify that longer recordings available from a subset of individuals did not make them easier to identify. We also correlated the root mean square (RMS) of signals that measured ocular, cardiac and head movement artifacts over the duration of the entire recording to participants' self-identifiability score. For cardiac artifacts for instance, we derived the RMS of ECG recordings; for ocular artifacts we used the HEOG and VEOG electrode recordings; and for motion artifact we extracted the RMS of all three head coil signals that measured 3-D head movements. These derivations were conducted for both the connectome and spectral broadband *within-session* fingerprinting challenge.

Fingerprinting across frequency bands

We replicated the above fingerprinting approach using data restricted to each frequency band of interest (delta 1-4Hz, theta 4-8Hz, alpha 8-13Hz, beta 13-30Hz, gamma 30-50Hz, and high gamma 50-150Hz). We report the identification accuracy obtained from each narrowband signal in both the spectral and connectome fingerprinting challenges in Figure 2 and Figure 3, for the *within-* and *between-session* fingerprinting challenges respectively.

Shortened and between-session fingerprinting challenges

We verified the robustness of MEG fingerprinting in relation to 1) the amount of data required to accurately identify individuals and 2) the stability of MEG identification across time. We subdivided participants into two additional challenges: the *within-session—shortened* and *between-session* challenge. First, we used the participant data described in the *within-session* analysis and extracted connectome and spectral fingerprinting features over three 30-second non-overlapping time segments. This duration was based on the length of the shortest recording in the data sample (Figure 1a_{ii}). We applied the same fingerprinting procedure as described in **Fingerprinting and self-identifiability** across all possible combinations of the three 30-second datasets. Second, we assessed the stability of the fingerprinting outcomes using a subset of participants with consecutive MEG sessions separated by several days (N=47; separated on average by 201.7 days, see Supplemental Materials for details). Again, we applied the same fingerprinting procedure as described in **Fingerprinting and self-identifiability** for this *between-session* challenge.

Most characteristic features for fingerprinting

We quantified the contribution of each feature (i.e., edges in the connectivity matrix or a frequency band in an anatomical parcel) towards identifying individuals using Intra-Class Correlations (ICC). ICC is commonly used to measure the agreement between two observers (e.g., ratings vs. scores). The stronger the agreement, the higher the ICC (12, 37). ICC derives a random effects model whereby each item is rated by different raters from a pool of potential raters. We selected this measure to capture the inter-rater reliability of each participant as their

own rater to identify which edges (e.g., connections in FC) are the most consistent (i.e., which features of a participant P_i in dataset 1 are most like dataset 2). Here, the higher the ICC, the more consistent a given feature was within individuals. Additionally, we computed two other measures of edgewise contribution proposed by Finn and colleagues (14): *group consistency* and *differential power* (Supplemental Material). We applied all measures (i.e., ICC, group consistency, and differential power) in the context of the broadband *within-session* fingerprinting challenge.

Partial Least-Squares: MEG features of participant demographics

We conducted a Partial Least-Squares (PLS) analysis with the Rotman-Baycrest PLS toolbox (71). PLS is a multivariate statistical method that relates two matrices of variables (e.g., neural activity and participant demographics) by estimating a weighted linear combination of variables from both data matrices to maximize their covariance. The associated weights can be interpreted neural patterns (e.g., functional connections) and their associated demographic profiles. PLS used singular value decompositions of the z-scored neural activity-demographics covariance matrix. This decomposition yielded orthogonal latent variables (LV) associated to a pattern of neural activity (i.e., functional connectivity or spectral power) and demographics. To assess the significance of these multivariate patterns, we computed permutation tests (10,000 permutations). Each permutation shuffled the order of the observations (i.e., the rows) of the demographic data matrix before running PLS on the resulting surrogate data under the null hypothesis that there was no relationship between the demographic and neural data. A p -value for the LVs was computed as the proportion of times the permuted singular values exceeded that of the original data. We explored the first significant LV from the broadband connectome and spectral fingerprinting features. We also assessed the contribution of each variable in the demographics and neural activity matrices by bootstrapping observations with replacement (10,000 bootstraps). We computed 95-% confidence intervals for the demographic weights and bootstrap ratios for the neural weights. The bootstrap ratio was computed as the ratio between each variable's weight and the bootstrap-estimated standard error.

Author Contribution

All authors conceptualized the study, J.D.S.C. and H.D.O. performed the analyses, S.B. and B.M. provided guidance with data interpretation, J.D.S.C. wrote the first draft of the manuscript, all authors contributed to the writing and editing of the manuscript.

Competing Interests

The authors declare no competing financial interest.

References

1. J. Dubois, R. Adolphs, Building a Science of Individual Differences from fMRI. *Trends Cogn. Sci.* **20**, 425–443 (2016).

- 550 2. M. B. Miller, J. D. Van Horn, Individual variability in brain activations associated with episodic
551 retrieval: a role for large-scale databases. *Int. J. Psychophysiol. Off. J. Int. Organ. Psychophysiol.* **63**,
552 205–213 (2007).
- 553 3. J. D. Van Horn, S. T. Grafton, M. B. Miller, Individual Variability in Brain Activity: A Nuisance or an
554 Opportunity? *Brain Imaging Behav.* **2**, 327 (2008).
- 555 4. T. Yarkoni, in *APA handbook of personality and social psychology, Volume 4: Personality processes*
556 *and individual differences.*, M. Mikulincer, P. R. Shaver, M. L. Cooper, R. J. Larsen, Eds. (American
557 Psychological Association, Washington, 2015; <http://content.apa.org/books/14343-002>), pp. 61–83.
- 558 5. D. S. Marcus, J. Harwell, T. Olsen, M. Hodge, M. F. Glasser, F. Prior, M. Jenkinson, T. Laumann, S. W.
559 Curtiss, D. C. Van Essen, Informatics and data mining tools and strategies for the human connectome
560 project. *Front. Neuroinformatics.* **5**, 4 (2011).
- 561 6. G. Niso, C. Rogers, J. T. Moreau, L.-Y. Chen, C. Madjar, S. Das, E. Bock, F. Tadel, A. C. Evans, P.
562 Jolicoeur, S. Baillet, OMEGA: The Open MEG Archive. *NeuroImage.* **124**, 1182–1187 (2016).
- 563 7. R. A. Poldrack, K. J. Gorgolewski, Making big data open: data sharing in neuroimaging. *Nat. Neurosci.*
564 **17**, 1510–1517 (2014).
- 565 8. R. B. Mars, R. E. Passingham, S. Jbabdi, Connectivity Fingerprints: From Areal Descriptions to Abstract
566 Spaces. *Trends Cogn. Sci.* **22**, 1026–1037 (2018).
- 567 9. B. Mišić, O. Sporns, From regions to connections and networks: new bridges between brain and
568 behavior. *Curr. Opin. Neurobiol.* **40**, 1–7 (2016).
- 569 10. S. A. Valizadeh, F. Liem, S. Méridat, J. Hänggi, L. Jäncke, Identification of individual subjects on the
570 basis of their brain anatomical features. *Sci. Rep.* **8**, 5611 (2018).
- 571 11. C. Wachinger, P. Golland, W. Kremen, B. Fischl, M. Reuter, BrainPrint: A discriminative
572 characterization of brain morphology. *NeuroImage.* **109**, 232–248 (2015).
- 573 12. E. Amico, J. Goñi, The quest for identifiability in human functional connectomes. *Sci. Rep.* **8**, 8254
574 (2018).
- 575 13. S. Bari, E. Amico, N. Vike, T. M. Talavage, J. Goñi, Uncovering multi-site identifiability based on
576 resting-state functional connectomes. *NeuroImage.* **202**, 115967 (2019).
- 577 14. E. S. Finn, X. Shen, D. Scheinost, M. D. Rosenberg, J. Huang, M. M. Chun, X. Papademetris, R. T.
578 Constable, Functional connectome fingerprinting: identifying individuals using patterns of brain
579 connectivity. *Nat. Neurosci.* **18**, 1664–1671 (2015).
- 580 15. T. Kaufmann, D. Alnæs, N. T. Doan, C. L. Brandt, O. A. Andreassen, L. T. Westlye, Delayed stabilization
581 and individualization in connectome development are related to psychiatric disorders. *Nat.*
582 *Neurosci.* **20**, 513–515 (2017).

- 583 16. O. Miranda-Dominguez, B. D. Mills, S. D. Carpenter, K. A. Grant, C. D. Kroenke, J. T. Nigg, D. A. Fair,
584 Connectotyping: model based fingerprinting of the functional connectome. *PloS One*. **9**, e111048
585 (2014).
- 586 17. M. Fraschini, A. Hillebrand, M. Demuru, L. Didaci, G. L. Marcialis, An EEG-Based Biometric System
587 Using Eigenvector Centrality in Resting State Brain Networks. *IEEE Signal Process. Lett.* **22**, 666–670
588 (2015).
- 589 18. W. Kong, L. Wang, S. Xu, F. Babiloni, H. Chen, EEG Fingerprints: Phase Synchronization of EEG Signals
590 as Biomarker for Subject Identification. *IEEE Access*. **7**, 121165–121173 (2019).
- 591 19. J. de Souza Rodrigues, F. L. Ribeiro, J. R. Sato, R. C. Mesquita, C. E. B. Júnior, Identifying individuals
592 using fNIRS-based cortical connectomes. *Biomed. Opt. Express*. **10**, 2889–2897 (2019).
- 593 20. A. S. Greene, S. Gao, D. Scheinost, R. T. Constable, Task-induced brain state manipulation improves
594 prediction of individual traits. *Nat. Commun.* **9**, 2807 (2018).
- 595 21. M. D. Rosenberg, D. Scheinost, A. S. Greene, E. W. Avery, Y. H. Kwon, E. S. Finn, R. Ramani, M. Qiu,
596 R. T. Constable, M. M. Chun, Functional connectivity predicts changes in attention observed across
597 minutes, days, and months. *Proc. Natl. Acad. Sci. U. S. A.* **117**, 3797–3807 (2020).
- 598 22. M. Yamashita, Y. Yoshihara, R. Hashimoto, N. Yahata, N. Ichikawa, Y. Sakai, T. Yamada, N.
599 Matsukawa, G. Okada, S. C. Tanaka, K. Kasai, N. Kato, Y. Okamoto, B. Seymour, H. Takahashi, M.
600 Kawato, H. Imamizu, A prediction model of working memory across health and psychiatric disease
601 using whole-brain functional connectivity. *eLife*. **7** (2018), doi:10.7554/eLife.38844.
- 602 23. K. Yoo, M. D. Rosenberg, W.-T. Hsu, S. Zhang, C.-S. R. Li, D. Scheinost, R. T. Constable, M. M. Chun,
603 Connectome-based predictive modeling of attention: Comparing different functional connectivity
604 features and prediction methods across datasets. *NeuroImage*. **167**, 11–22 (2018).
- 605 24. E. Bullmore, O. Sporns, The economy of brain network organization. *Nat. Rev. Neurosci.* **13**, 336–349
606 (2012).
- 607 25. S. M. Smith, D. Vidaurre, C. F. Beckmann, M. F. Glasser, M. Jenkinson, K. L. Miller, T. E. Nichols, E. C.
608 Robinson, G. Salimi-Khorshidi, M. W. Woolrich, D. M. Barch, K. Uğurbil, D. C. Van Essen, Functional
609 connectomics from resting-state fMRI. *Trends Cogn. Sci.* **17**, 666–682 (2013).
- 610 26. S. Baillet, Magnetoencephalography for brain electrophysiology and imaging. *Nat. Neurosci.* **20**,
611 327–339 (2017).
- 612 27. E. Başar, *Chaos in Brain Function: Containing Original Chapters by E. Basar and T. H. Bullock and*
613 *Topical Articles Reprinted from the Springer Series in Brain Dynamics* (Springer Science & Business
614 Media, 1990).
- 615 28. R. B. Stein, E. R. Gossen, K. E. Jones, Neuronal variability: noise or part of the signal? *Nat. Rev.*
616 *Neurosci.* **6**, 389–397 (2005).
- 617 29. L. Q. Uddin, Bring the Noise: Reconceptualizing Spontaneous Neural Activity. *Trends Cogn. Sci.* **24**,
618 734–746 (2020).

- 619 30. E. Florin, S. Baillet, The brain's resting-state activity is shaped by synchronized cross-frequency
620 coupling of neural oscillations. *NeuroImage*. **111**, 26–35 (2015).
- 621 31. L. Iemi, N. A. Busch, A. Laudini, S. Haegens, J. Samaha, A. Villringer, V. V. Nikulin, Multiple
622 mechanisms link prestimulus neural oscillations to sensory responses. *eLife*. **8** (2019),
623 doi:10.7554/eLife.43620.
- 624 32. J. Samaha, L. Iemi, S. Haegens, N. A. Busch, Spontaneous Brain Oscillations and Perceptual Decision-
625 Making. *Trends Cogn. Sci.* **24**, 639–653 (2020).
- 626 33. S. Bodenmann, T. Rusterholz, R. Dürr, C. Stoll, V. Bachmann, E. Geissler, K. Jaggi-Schwarz, H.-P.
627 Landolt, The functional Val158Met polymorphism of COMT predicts interindividual differences in
628 brain alpha oscillations in young men. *J. Neurosci. Off. J. Soc. Neurosci.* **29**, 10855–10862 (2009).
- 629 34. S. Haegens, H. Cousijn, G. Wallis, P. J. Harrison, A. C. Nobre, Inter- and intra-individual variability in
630 alpha peak frequency. *NeuroImage*. **92**, 46–55 (2014).
- 631 35. S. Baillet, J. C. Mosher, R. M. Leahy, Electromagnetic brain mapping. *IEEE Signal Process. Mag.* **18**,
632 14–30 (2001).
- 633 36. R. S. Desikan, F. Ségonne, B. Fischl, B. T. Quinn, B. C. Dickerson, D. Blacker, R. L. Buckner, A. M. Dale,
634 R. P. Maguire, B. T. Hyman, M. S. Albert, R. J. Killiany, An automated labeling system for subdividing
635 the human cerebral cortex on MRI scans into gyral based regions of interest. *NeuroImage*. **31**, 968–
636 980 (2006).
- 637 37. P. E. Shrout, J. L. Fleiss, Intraclass correlations: Uses in assessing rater reliability. *Psychol. Bull.* **86**,
638 420–428 (1979).
- 639 38. B. T. Yeo, Thomas, F. M. Krienen, J. Sepulcre, M. R. Sabuncu, D. Lashkari, M. Hollinshead, J. L.
640 Roffman, J. W. Smoller, L. Zöllei, J. R. Polimeni, B. Fischl, H. Liu, R. L. Buckner, The organization of the
641 human cerebral cortex estimated by intrinsic functional connectivity. *J. Neurophysiol.* **106**, 1125–
642 1165 (2011).
- 643 39. S. Noble, M. N. Spann, F. Tokoglu, X. Shen, R. T. Constable, D. Scheinost, Influences on the Test-
644 Retest Reliability of Functional Connectivity MRI and its Relationship with Behavioral Utility. *Cereb.*
645 *Cortex N. Y. N 1991*. **27**, 5415–5429 (2017).
- 646 40. J. Cabral, M. L. Kringelbach, G. Deco, Functional connectivity dynamically evolves on multiple time-
647 scales over a static structural connectome: Models and mechanisms. *NeuroImage*. **160**, 84–96
648 (2017).
- 649 41. M. Nentwich, L. Ai, J. Madsen, Q. K. Telesford, S. Haufe, M. P. Milham, L. C. Parra, Functional
650 connectivity of EEG is subject-specific, associated with phenotype, and different from fMRI.
651 *NeuroImage*. **218**, 117001 (2020).
- 652 42. C. L. Horien, X. Shen, D. Scheinost, R. T. Constable, The individual functional connectome is unique
653 and stable over months to years. *Neuroimage* (2019), doi:10.1016/j.neuroimage.2019.02.002.

- 654 43. M. J. Brookes, M. Woolrich, H. Luckhoo, D. Price, J. R. Hale, M. C. Stephenson, G. R. Barnes, S. M.
655 Smith, P. G. Morris, Investigating the electrophysiological basis of resting state networks using
656 magnetoencephalography. *Proc. Natl. Acad. Sci. U. S. A.* **108**, 16783–16788 (2011).
- 657 44. B. A. E. Hunt, P. K. Tewarie, O. E. Mougin, N. Geades, D. K. Jones, K. D. Singh, P. G. Morris, P. A.
658 Gowland, M. J. Brookes, Relationships between cortical myeloarchitecture and electrophysiological
659 networks. *Proc. Natl. Acad. Sci.* **113**, 13510 (2016).
- 660 45. G. Michalareas, J. Vezoli, S. van Pelt, J.-M. Schoffelen, H. Kennedy, P. Fries, Alpha-Beta and Gamma
661 Rhythms Subserve Feedback and Feedforward Influences among Human Visual Cortical Areas.
662 *Neuron.* **89**, 384–397 (2016).
- 663 46. B. Morillon, S. Baillet, Motor origin of temporal predictions in auditory attention. *Proc. Natl. Acad.*
664 *Sci.* **114**, E8913–E8921 (2017).
- 665 47. S. Haufe, P. DeGuzman, S. Henin, M. Arcaro, C. J. Honey, U. Hasson, L. C. Parra, Elucidating relations
666 between fMRI, ECoG, and EEG through a common natural stimulus. *NeuroImage.* **179**, 79–91 (2018).
- 667 48. N. K. Logothetis, J. Pauls, M. Augath, T. Trinath, A. Oeltermann, Neurophysiological investigation of
668 the basis of the fMRI signal. *Nature.* **412**, 150–157 (2001).
- 669 49. J. F. Nottage, J. Horder, State-of-the-Art Analysis of High-Frequency (Gamma Range)
670 Electroencephalography in Humans. *Neuropsychobiology.* **72**, 219–228 (2015).
- 671 50. E. M. Whitham, K. J. Pope, S. P. Fitzgibbon, T. Lewis, C. R. Clark, S. Loveless, M. Broberg, A. Wallace,
672 D. DeLosAngeles, P. Lillie, A. Hardy, R. Fronsco, A. Pulbrook, J. O. Willoughby, Scalp electrical
673 recording during paralysis: Quantitative evidence that EEG frequencies above 20Hz are
674 contaminated by EMG. *Clin. Neurophysiol.* **118**, 1877–1888 (2007).
- 675 51. S. Yuval-Greenberg, O. Tomer, A. S. Keren, I. Nelken, L. Y. Deouell, Transient induced gamma-band
676 response in EEG as a manifestation of miniature saccades. *Neuron.* **58**, 429–441 (2008).
- 677 52. Y. Bagherzadeh, D. Baldauf, D. Pantazis, R. Desimone, Alpha Synchrony and the Neurofeedback
678 Control of Spatial Attention. *Neuron.* **105**, 577-587.e5 (2020).
- 679 53. M. S. Clayton, N. Yeung, R. Cohen Kadosh, The many characters of visual alpha oscillations. *Eur. J.*
680 *Neurosci.* **48**, 2498–2508 (2018).
- 681 54. J. J. Foster, E. Awh, The role of alpha oscillations in spatial attention: limited evidence for a
682 suppression account. *Curr. Opin. Psychol.* **29**, 34–40 (2019).
- 683 55. M. D. Rosenberg, E. S. Finn, D. Scheinost, X. Papademetris, X. Shen, R. T. Constable, M. M. Chun, A
684 neuromarker of sustained attention from whole-brain functional connectivity. *Nat. Neurosci.* **19**,
685 165–171 (2016).
- 686 56. M. D. Rosenberg, E. S. Finn, D. Scheinost, R. T. Constable, M. M. Chun, Characterizing Attention with
687 Predictive Network Models. *Trends Cogn. Sci.* **21**, 290–302 (2017).

- 688 57. T. Harmelech, R. Malach, Neurocognitive biases and the patterns of spontaneous correlations in the
689 human cortex. *Trends Cogn. Sci.* **17**, 606–615 (2013).
- 690 58. H. Cai, J. Zhu, Y. Yu, Robust prediction of individual personality from brain functional connectome.
691 *Soc. Cogn. Affect. Neurosci.* **15**, 359–369 (2020).
- 692 59. C. Parkinson, A. M. Kleinbaum, T. Wheatley, Similar neural responses predict friendship. *Nat.*
693 *Commun.* **9**, 332 (2018).
- 694 60. D. C. Glahn, A. M. Winkler, P. Kochunov, L. Almasy, R. Duggirala, M. A. Carless, J. C. Curran, R. L.
695 Olvera, A. R. Laird, S. M. Smith, C. F. Beckmann, P. T. Fox, J. Blangero, M. E. Raichle, Genetic Control
696 over the Resting Brain. *Proc. Natl. Acad. Sci. U. S. A.* **107**, 1223–1228 (2010).
- 697 61. M. S. Korgaonkar, K. Ram, L. M. Williams, J. M. Gatt, S. M. Grieve, Establishing the resting state
698 default mode network derived from functional magnetic resonance imaging tasks as an
699 endophenotype: A twins study. *Hum. Brain Mapp.* **35**, 3893–3902 (2014).
- 700 62. O. Miranda-Dominguez, E. Feczko, D. S. Grayson, H. Walum, J. T. Nigg, D. A. Fair, Heritability of the
701 human connectome: A connectotyping study. *Netw. Neurosci. Camb. Mass.* **2**, 175–199 (2018).
- 702 63. C. A. Hodgkinson, M.-A. Enoch, V. Srivastava, J. S. Cummins-Oman, C. Ferrier, P. Iarikova, S.
703 Sankararaman, G. Yamini, Q. Yuan, Z. Zhou, B. Albaugh, K. V. White, P.-H. Shen, D. Goldman,
704 Genome-wide association identifies candidate genes that influence the human
705 electroencephalogram. *Proc. Natl. Acad. Sci. U. S. A.* **107**, 8695–8700 (2010).
- 706 64. E. Leppäaho, H. Renvall, E. Salmela, J. Kere, R. Salmelin, S. Kaski, Discovering heritable modes of MEG
707 spectral power. *Hum. Brain Mapp.* **40**, 1391–1402 (2019).
- 708 65. E. Salmela, H. Renvall, J. Kujala, O. Hakosalo, M. Illman, M. Vihla, E. Leinonen, R. Salmelin, J. Kere,
709 Evidence for genetic regulation of the human parieto-occipital 10-Hz rhythmic activity. *Eur. J.*
710 *Neurosci.* **44**, 1963–1971 (2016).
- 711 66. F. Tadel, S. Baillet, J. C. Mosher, D. Pantazis, R. M. Leahy, Brainstorm: a user-friendly application for
712 MEG/EEG analysis. *Comput. Intell. Neurosci.* **2011**, 879716 (2011).
- 713 67. J. Gross, S. Baillet, G. R. Barnes, R. N. Henson, A. Hillebrand, O. Jensen, K. Jerbi, V. Litvak, B. Maess,
714 R. Oostenveld, L. Parkkonen, J. R. Taylor, V. van Wassenhove, M. Wibral, J.-M. Schoffelen, Good
715 practice for conducting and reporting MEG research. *NeuroImage.* **65**, 349–363 (2013).
- 716 68. B. Fischl, FreeSurfer. *NeuroImage.* **62**, 774–781 (2012).
- 717 69. A. Bruns, R. Eckhorn, H. Jokeit, A. Ebner, Amplitude envelope correlation detects coupling among
718 incoherent brain signals. *Neuroreport.* **11**, 1509–1514 (2000).
- 719 70. P. Welch, The use of fast Fourier transform for the estimation of power spectra: A method based on
720 time averaging over short, modified periodograms. *IEEE Trans. Audio Electroacoustics.* **15**, 70–73
721 (1967).

71. A. R. McIntosh, N. J. Lobaugh, Partial least squares analysis of neuroimaging data: applications and advances. *NeuroImage*. **23 Suppl 1**, S250-263 (2004).

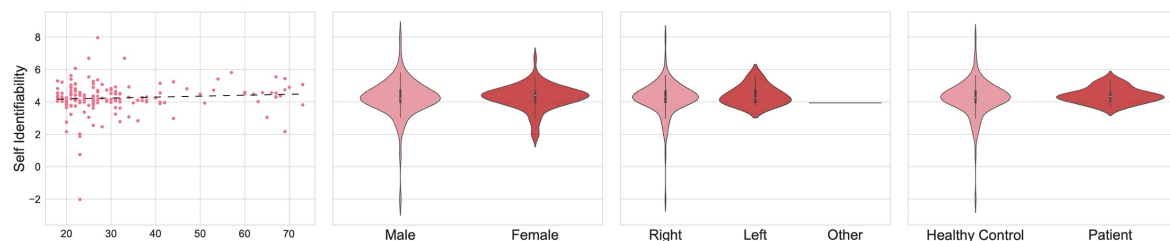
Supplemental material

MEG fingerprinting is robust against sample demographics

The OMEGA data repository contains 158 participants, with a subset (N=47) scanned at multiple occasions several days apart. OMEGA consists essentially of data from healthy controls with a 18-73-year age span (SD=14.7 years; Supplemental Table 1).

One potential confound that could have inflated our ability to fingerprint individuals is the heterogeneity introduced by both healthy and clinical populations in the OMEGA cohort. To address this concern, we ran a secondary analysis where we performed the fingerprinting procedures described in the manuscript with only healthy controls (N=130). The results, reported in Supplemental Table 2, demonstrated that fingerprint performances were not biased by the patients/controls heterogeneity of the OMEGA sample. We observed a decrease of less than 1% in performance relative to fingerprinting from the entire cohort. Further, there was no clear relationship between self-identifiability and demographics (Figure S1)., using connectome (age: $r = 0.08$, $p = 0.2$; gender: $t = -0.27$, $p = 0.7$; handedness: $t = -0.51$, $p = 0.6$; clinical status: $t = -0.87$, $p = 0.3$; two-tailed) and spectral fingerprinting (age: $r = 0.10$, $p = 0.1$; gender: $t = 0.62$, $p = 0.5$; handedness: $t = 0.13$, $p = 0.8$; clinical status: $t = 0.84$, $p = 0.3$; two-tailed).

(a) Functional Connectivity



(b) Power Spectral Density



Figure S1: Self identifiability was not associated with demographics

The plots depict demographic variables and corresponding self-identifiability scores across both (a) connectome and (b) spectral broadband *within-session* fingerprinting. Demographic variables included age, biological sex, dominant hand, and healthy vs. patient categories. There was no clear

relationship between demographics and self-identifiability — i.e., differences in demographics did not drive self-identifiability.

Acquisition parameters did not affect either fingerprinting performances (Figure S2). Participants with longer recordings (i.e., more data) were not more identifiable (connectome: $r = -0.02$, $p = 0.7$; spectral: $r = 0.02$, $p = 0.8$). This observation is consistent with the *shortened within-session* fingerprinting results, which demonstrate individuals were identifiable from shorter 30-second recordings (see below).

Taken together, these supplemental results demonstrate that MEG fingerprinting is robust against data artifacts, heterogeneous sample demographics and acquisition parameters.

	Within-session data	Between-session data
Age	31.9 ± 14.7	26.7 ± 11.6
Gender	77 Females	24 Females
Dominant Hand	147 Right, 8 Left, 1 Other	44 Right, 3 Left
Clinical Status	130 Healthy Controls 22 ADHD 6 Chronic Pain	25 Healthy Controls 22 ADHD

Supplemental table 1: OMEGA Participant Demographics

Demographic variables summarized for both subsets of the OMEGA data repository.

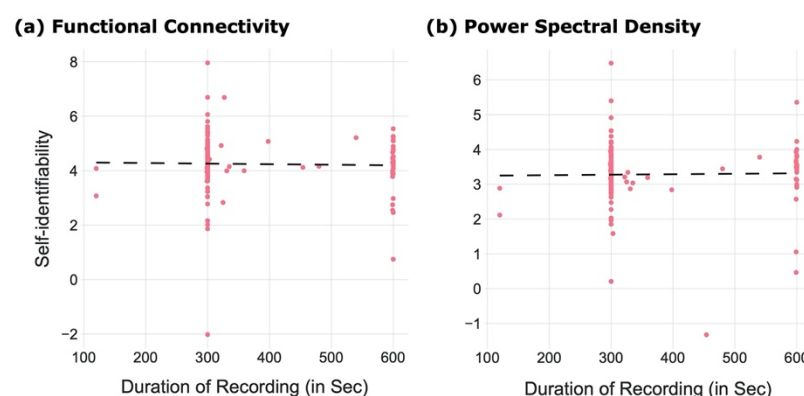


Figure S2: Recording duration did not affect self-identifiability

Scatter plots of self-identifiability vs. duration of data collections, for the broadband *within-session* challenge. There was no clear relationship between self-identifiability and the duration of the MEG recordings across participants.

	All Participants		Only Healthy Controls	
	Dataset 1 to Dataset 2	Dataset 2 to Dataset 1	Dataset 1 to Dataset 2	Dataset 2 to Dataset 1
Connectome	94.9%	94.3%	93.8%	93.0%
Spectral	96.2%	96.2%	95.3%	95.3%

Supplemental table 2. Fingerprinting performances of healthy controls

Identification performances of connectome and spectral broadband *within-session* fingerprinting obtained from for the entire repository (healthy controls and patients), and from healthy participants only. Each column reports fingerprinting performances from Dataset 1 to Dataset 2 and vice-versa (see Figure 1 for details). Overall, identification accuracy decreased slightly by ~0.9% when comprising healthy participants only. Consistent with our findings reported in Figure S2, clinical status did not play a major role in the identification of individuals.

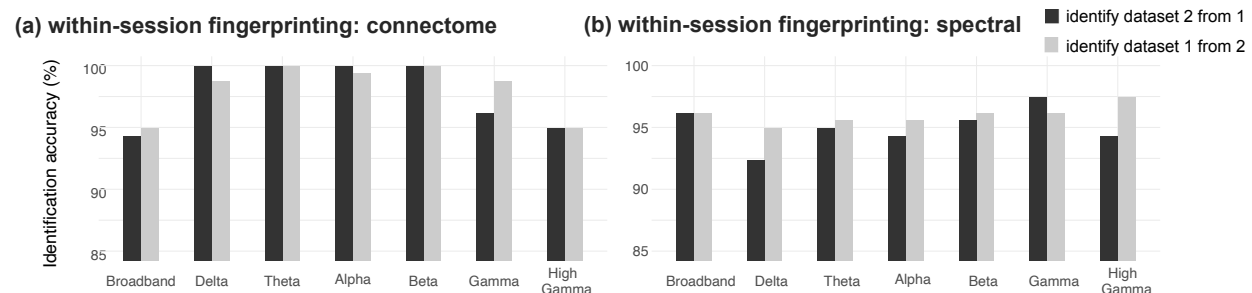


Figure S3: Identification accuracy from within-session datasets

Results from MEG *within-session* fingerprinting. Identification accuracy for (a) connectome and (b) spectral fingerprinting (broadband and narrowband data). The accuracy scores are reported for identification from dataset 1 to dataset 2 and vice-versa, as explained in Methods.

PCA reconstruction does little to improve MEG fingerprinting

Amico and Goñi (1) previously reported improvements to participant differentiation when using data reduction techniques prior to identification, using e.g., principal component analysis (PCA). We reproduced their approach, using PCA to reduce the dimensionality of the connectome and spectral feature spaces prior to fingerprinting. Our results provided little support to PCA reconstruction improving identification accuracy, as shown Figure S4 and in Supplemental Table 3. PCA increased self-identifiability by less than 1.5%. Data reduction had limited beneficial impact possibly because of high fingerprinting performances at baseline (without data reduction). We also emphasize that we conducted MEG source time series extraction via a PCA of all local time

series within each parcel. It is therefore likely that this dimension reduction procedure contributed to improve signal-to-noise ratio and limited the impact of subsequent PCA of features.

	Original (un-reconstructed)		PCA Reconstructed	
	Dataset 1 to Dataset 2	Dataset 2 to Dataset 1	Dataset 1 to Dataset 2	Dataset 2 to Dataset 1
Connectome	94.9%	94.3%	96.2%	96.2%
Spectral	96.2%	96.2%	96.2%	96.2%

Supplemental Table 3: PCA reconstruction did not improve accuracy

Performances in identification accuracy for connectome and spectral broadband *within-session* fingerprinting, for both original and PCA-reconstructed data (1). PCA data reduction improved connectome fingerprinting performances only slightly (about 2%). It had virtually no effect on spectral fingerprinting performances.

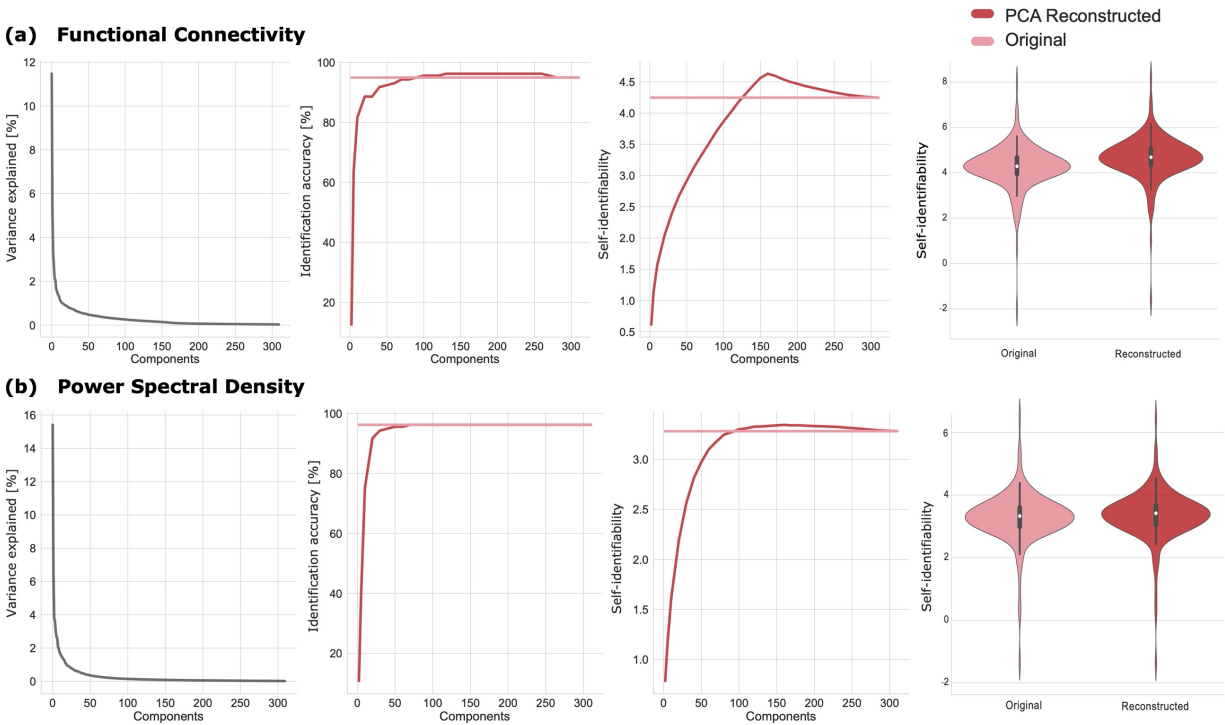


Figure S4: Limited benefit of PCA reconstruction on identification accuracy

PCA reconstruction as proposed by Amico and Goñi (2018) had limited effect on (a) connectome and (b) spectral *within-session* fingerprinting. The original results (Figure 2) are plotted against PCA-reconstructed results. From left to right, plots show i) PCA components plotted vs. their

respective fractions of signal variance explained, *ii*) identification accuracy across PCA components, *iii*) average self-identifiability across PCA components, and *iv*) violin plots of self-identifiability before and after PCA reconstruction. Overall, PCA reconstruction did not substantially improve identification accuracy.

Fingerprinting with 30 second data segments and across recording sessions

We challenged MEG fingerprinting using short 30-second data segments (i.e., shortened *within-session* fingerprinting). We epoched participants' MEG recordings into three datasets of 30 second, where the first dataset was the first 30 seconds of the recording after having removed the initial five seconds, the second dataset was the 30 seconds immediately following the first dataset, and the last dataset was the last 30-second segment of the recording after having removed the last ten seconds (Figure 1). Cropping the initial and last few seconds from recordings excluded edge filtering and other session artifacts. The lengths of the short datasets and epochs were determined from the participant with the shortest available recording. This procedure yielded three data segments for fingerprinting purposes via 6 possible dataset pairs (i.e., dataset 1 and 2; dataset 2 and 3; and dataset 1 and 3 and vice-versa). Results for all possible combinations of datasets are reported in Figure S5.

Remarkably, connectome fingerprinting successfully identified individuals across all possible combinations of datasets regardless of their proximity in time (Figure S5). Spectral fingerprinting yielded lower identification accuracy than connectome fingerprinting, specifically when the datasets were further apart in time (i.e., dataset 1 and 3). This outcome is discussed in the main manuscript.

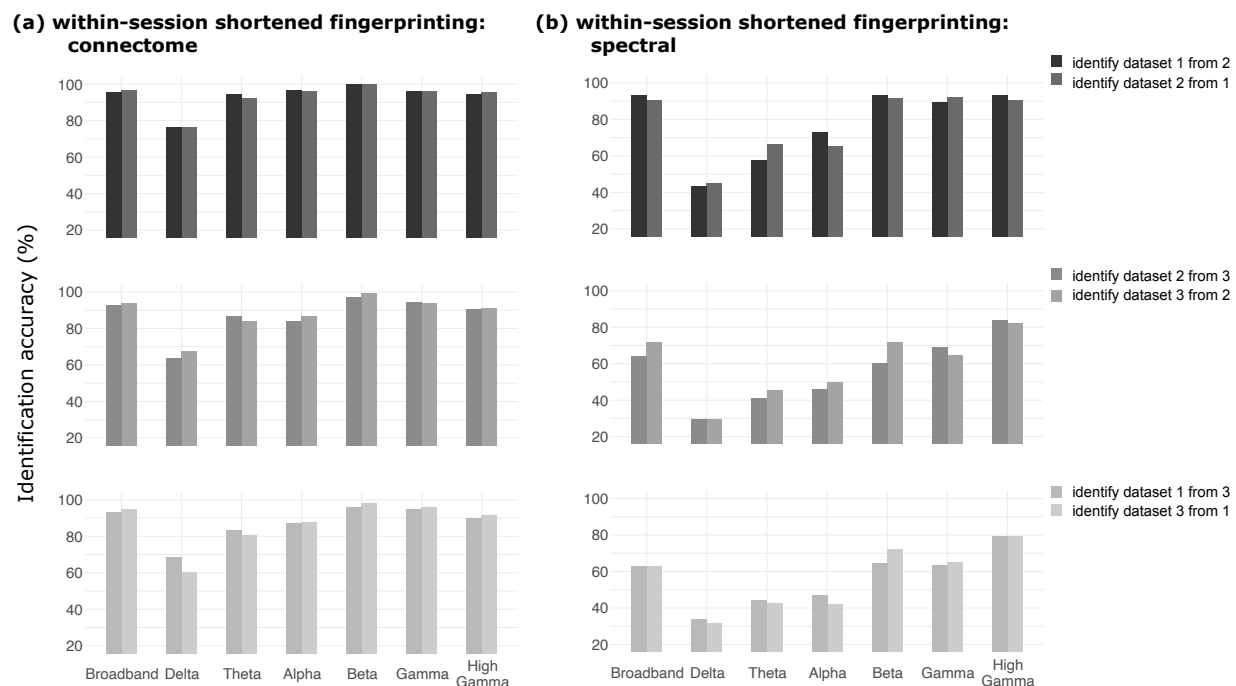


Figure S5: Identification accuracy from shortened within-session datasets

Identification results from shortened *within-session* datasets (30 seconds) for (a) connectome and (b) spectral broadband and narrowband fingerprinting. The accuracy scored are reported for identification from all possible combinations of datasets, (i.e., dataset 1 to predict dataset 2, dataset 3 to predict dataset 2, etc.; see Methods for details). Identification accuracy increased as datasets were proximal in time (i.e., fingerprinting accuracy for dataset 1 to dataset 2 was greater than for dataset 1 to dataset 3).

In a similar fashion, we also report the fingerprinting accuracy performances for all possible pairs of datasets for the *between-session* fingerprinting challenge in Figure S6. Overall, spectral fingerprinting outperformed connectome fingerprinting, as discussed in the main text.

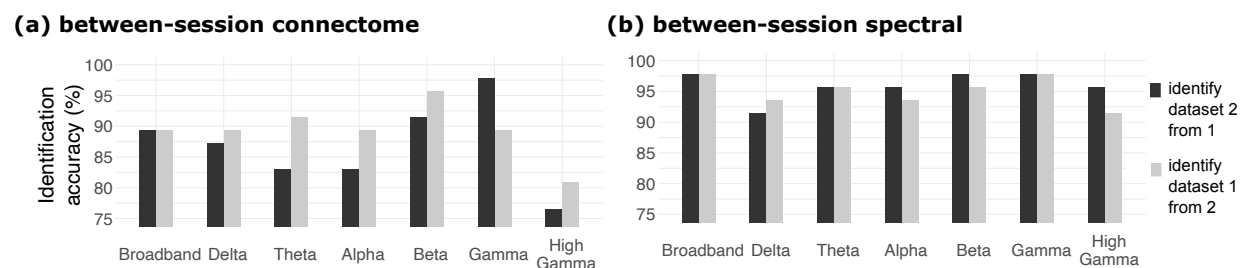


Figure S6: Between-session identification accuracy

Results from MEG *between-session* fingerprinting. Identification accuracy for both (a) connectome and (b) spectral broadband and narrowband fingerprinting. The accuracy scores are reported for identification from dataset 1 to dataset 2 and vice-versa (see Methods).

Salient neurophysiological features for fingerprinting

We reported in the main manuscript intraclass correlations (ICC) to determine which features contributed to individual identification the most. We also performed two additional analyses, deriving *group consistency* and *differential power*. These two metrics were proposed by Finn and colleagues (2) to identify the features which were the most consistent across their cohort, vs. The features which were the most consistent within individuals but different across participant, respectively (2). Differential power measures the empirical probability that a given feature is more likely to have a higher edgewise product vector across individuals than within the same individual. Taking the sum of the natural log of this probability across subjects yields differential power (2). The higher the differential power, the better a feature discriminates between individuals. Results for differential power are plotted in Figures S7 and S9. We found that the most discriminant connectome features were the visual and limbic networks across frequency bands, while the most discriminant spectral features remained along midline structures for fast oscillatory signal components. Overall, these results confirmed the ICC analysis results, with the addition of the contributions of spectral power in the beta and gamma band along the supplementary motor, motor, and somatosensory cortices.

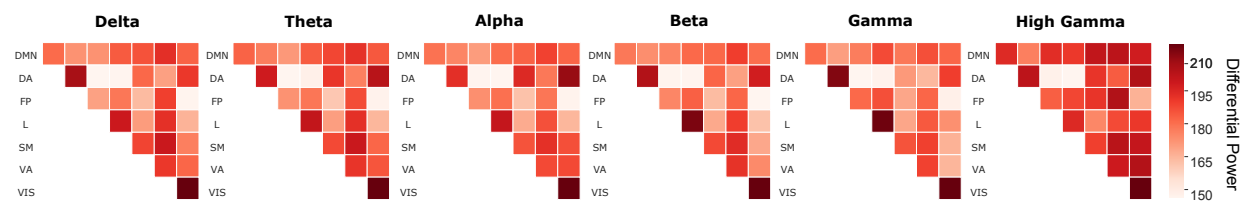


Figure S7: Differential Power Connectome Fingerprinting

Differential Power (DP) analysis for broadband connectome fingerprinting of the *within-session* dataset (see Figure 1). Mean DP plotted within frequency bands and per resting-state network as defined by (3): Default Mode Network (DMN), Dorsal Attention (DA), Frontal-Parietal (FP), Limbic (L), Somato-Motor (SM), Ventral Attention (VA), and Visual (VIS). The higher the DP, the more the corresponding functional connection was essential for fingerprinting. The outstanding connections determined by DP for fingerprinting were the Visual network across all frequency bands, and the Limbic network in the beta and gamma bands.

Group consistency reflects edges that are consistent across individuals. Group consistency was computed from the mean edgewise product vector across all subjects (2). Large values of group consistency highlight features that are consistent both within participants and across the cohort. Our analyses are shown Figures S8 and S10. The resulting most consistent connectome features remained along the diagonal of the FC matrix (i.e., connections within the same networks) specifically in the Dorsal Attention and Fronto-Parietal networks. The most consistent features for spectral fingerprinting were in the lower frequency bands, specifically in the lateral frontal cortices. This outcome was consistent with our ICC results (see Manuscript).

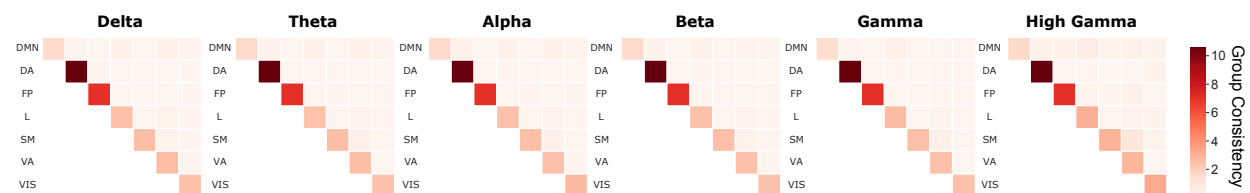


Figure S8: Group Consistency Connectome Fingerprinting

Group Consistency (GC) analysis for broadband connectome fingerprinting of the *within-session* dataset (see Figure 1). Mean GC plotted within frequency bands according to the labels from (3): Default Mode Network (DMN), Dorsal Attention (DA), Frontal-Parietal (FP), Limbic (L), Somato-Motor (SM), Ventral Attention (VA), and Visual (VIS). The higher the GC, the more consistent was a functional connection within an individual and across the cohort. The most consistent connections were those along the diagonal, specifically for the Dorsal Attention and Frontal-Parietal networks across all frequency bands.

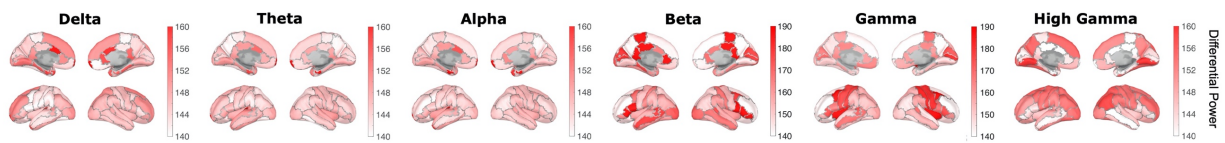


Figure S9: Differential Power Spectral Fingerprinting

Differential Power (DP) analysis for broadband spectral fingerprinting of the *within-session* dataset (see Figure 1). Mean DP plotted within frequency bands according to the Desikan-Killiany atlas (4). The higher the DP, the more a given frequency band and ROI distinguished between individuals. The most characteristic regions and frequencies were medial structures for the beta band, and temporal and central regions for gamma band signals.

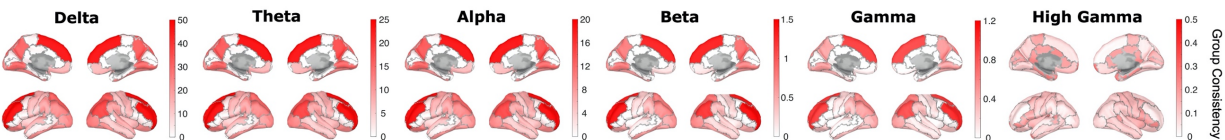


Figure S10: Group Consistency Spectral Fingerprinting

Group Consistency (GC) analyses for broadband spectral fingerprinting of the *within recording session* dataset (see Figure 1). Mean GC plotted within frequency bands according to the Desikan-Killiany atlas (4). The higher the GC, the more a given frequency band and ROI remained consistent within individuals and across the cohort. The most stable frequencies were the lower bands (delta and theta) and the most consistent regions across individuals were lateral frontal areas.

Partial Least Squares (PLS) analysis

We tested whether differences in resting-state neurophysiological signals related to meaningful demographic features using an exploratory Partial Least Squares (PLS) analysis. PLS is a multivariate statistical method that relates two data matrices based on latent variables (LV) that explain the highest covariance between the two datasets. Here, our two datasets consist of a demographic matrix (i.e., age, gender, handedness, and clinical status) and a neurophysiological data matrix (i.e., spectral power or functional connectome). Latent variables (which explain the most covariance between both matrices), and their corresponding variance explained are plotted in Figure S11. Significance of each latent variable was assessed via permutation tests. Permuting the rows of the data allowed us to compute an associate p-value for each latent variable (see Manuscript). We chose to explore the first significant latent variable which explained the most variance for each neurophysiological signal feature (i.e., the first component for connectomes and spectral data). The resulting weights associated to the latent neural and demographic components are depicted Figure 5 along with their bootstrapped ratios. These results corroborate how

neurophysiological signals at rest, in addition to identifying individuals, carry meaningful information about participant demographics.

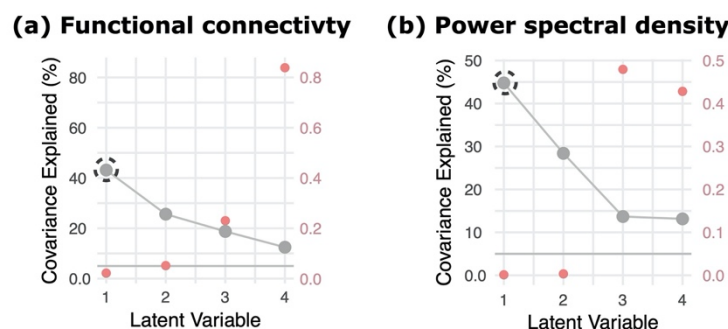


Figure S11: PLS latent variables

Results for the PLS analysis conducted for both (a) connectome and (b) spectral fingerprinting features. Each plot depicts the latent components obtained for each of the PLS analyses, their corresponding variance explained, and permuted p -value (right axis). One significant latent variable explained 43.1% of the variance for connectome fingerprinting and two latent variables explained 44.7% and 28.3% of the variance for spectral fingerprinting, respectively. We explored in the main Manuscript only the first significant component for each method (i.e., the circled component).

References

1. E. Amico, J. Goñi, The quest for identifiability in human functional connectomes. *Sci. Rep.* **8**, 8254 (2018).
2. E. S. Finn, X. Shen, D. Scheinost, M. D. Rosenberg, J. Huang, M. M. Chun, X. Papademetris, R. T. Constable, Functional connectome fingerprinting: identifying individuals using patterns of brain connectivity. *Nat. Neurosci.* **18**, 1664–1671 (2015).
3. B. T. Yeo, Thomas, F. M. Krienen, J. Sepulcre, M. R. Sabuncu, D. Lashkari, M. Hollinshead, J. L. Roffman, J. W. Smoller, L. Zöllei, J. R. Polimeni, B. Fischl, H. Liu, R. L. Buckner, The organization of the human cerebral cortex estimated by intrinsic functional connectivity. *J. Neurophysiol.* **106**, 1125–1165 (2011).
4. R. S. Desikan, F. Ségonne, B. Fischl, B. T. Quinn, B. C. Dickerson, D. Blacker, R. L. Buckner, A. M. Dale, R. P. Maguire, B. T. Hyman, M. S. Albert, R. J. Killiany, An automated labeling system for subdividing the human cerebral cortex on MRI scans into gyral based regions of interest. *NeuroImage*. **31**, 968–980 (2006).